Unraveling the composition dependence of the martensitic transformation temperature: A first-principles study of Ti-Ta alloys

Tanmoy Chakraborty,* Jutta Rogal, and Ralf Drautz
Interdisciplinary Centre for Advanced Materials Simulation, Ruhr-Universität Bochum, 44780 Bochum, Germany
(Received 21 October 2016; published 19 December 2016)

The martensitic start temperature M_s is one of the key characteristics of shape memory materials. High-temperature shape memory alloys are a special class of materials where transformation temperatures between the martensite and austenite phase above 373 K are desirable. For the design of new high-temperature shape memory alloys it is therefore important to understand and predict the dependence of M_s on the composition of the material. Using density functional theory in combination with the quasiharmonic Debye model, we evaluate the different contributions to the free energy to determine the transition temperature T_0 over a wide range of compositions in Ti-Ta alloys. Our approach provides physical insight into the various contributions that explain the strong composition dependence of M_s that is observed experimentally. Based on our calculations, we identify the relative phase stability at $T = 0$ K and the vibrational entropy difference between the involved phases as critical parameters to predict changes in T_0. We propose a simple, one-dimensional descriptor to estimate the transition temperature that can be used in the identification of new alloys suitable for high-temperature shape memory applications.

DOI: 10.1103/PhysRevB.94.224104

I. INTRODUCTION

Due to a reversible martensitic transformation, shape memory alloys (SMAs) exhibit unique functional properties which can be used in sensors or actuators for automotive and aerospace industrial applications and many more [1–3]. In order to extend the applicability of SMAs to high temperatures, a high martensitic transformation temperature $M_s > 373$ K is required [1]. β-type Ti-base shape memory alloys such as Ti-Mo, Ti-Nb, Ti-Ta, etc., are a class of materials that do not only exhibit a high martensitic transformation temperature [4–6], but also show excellent cold workability [7], which makes them attractive as potential high-temperature SMAs (HTSMAs). In Ti-base SMAs, the reversible martentsitic transformation occurs between the cubic β phase (high-temperature austenite) and the orthorhombic α'' phase (low-temperature martensite). These alloys are sensitive to aging at intermediate temperatures (373–673 K), where the ω phase is formed in either a hexagonal or a trigonal crystal structure [8,9]. The ω phase can cause embrittlement and destroy the shape memory effect. The formation of the detrimental ω phase can be suppressed by β-stabilizing elements such as Mo, Nb, or Ta, where Ta was found to be most effective [2,10]. But the increase in β stabilizing elements also decreases M_s. When adding Ta, M_s decreases by 30 K at. %, for Nb M_s decreases by 40 K at. % [2,11]. Experimentally, Ti-32Ta has been confirmed to exhibit a stable shape memory effect with high M_s and is thus considered a suitable candidate for HTSMAs [2].

A detailed theoretical understanding of the composition dependence of M_s in Ti-Ta alloys is to the best of our knowledge still missing. Buenconsejo *et al.* performed experiments with ternary alloys keeping the Ta content at 30 at. %, where they again observed a decrease in M_s with an increase in alloying elements, but could not identify any correlation between M_s and the number of valence electrons per atom (e/a) [12]. Further parameters that have been discussed in literature include the austenite elastic properties [13–19]. In particular for Ni-Ti base SMAs these parameters have been discussed in detail. As an example, Ren *et al.* explained the composition dependence of the M_s in Ni-Ti alloys based on the elastic constants showing that C' and C_{44} both increase with the addition of Fe to Ni-Ti alloys [20], which improves the dynamical stability but lowers M_s. Another study of ternary and quaternary Ni-Ti alloys revealed that an increase in valence electron concentration (c_v) with additional alloying elements causes higher elastic moduli which ultimately decreases M_s [21]. Overall, these studies suggest that with a change in composition the elastic moduli change which in turn influence the M_s [22,23]. However, Frenzel *et al.* [24] showed in their study that it is not the change in valence electrons but the stabilization of the B2 phase by the formation of Ni-antisite defects that is the key parameter for explaining the concentration dependence of M_s in Ni-Ti binary alloys. For Ti-Ta HTSMAs, the picture is less clear and the aim of this study is to provide a more comprehensive understanding of the composition dependence of the transformation temperature in these alloys. In particular for the design of new alloys a simple descriptive parameter to estimate the transition temperature would be very useful.

Using density functional theory (DFT) calculations in combination with the quasiharmonic Debye model, we determine the free energies of the martensite and austenite phase in Ti-Ta alloys as a function of composition. From the free-energy differences we evaluate the transformation temperature T_0. The change in T_0 as a function of composition is in excellent agreement with experimentally measured values of M_s. From the analysis of our calculations we identify the relative phase stability at $T = 0$ K and the difference in the vibrational entropy of the involved phases as the two key parameters in predicting the composition dependence of T_0. These two parameters can be combined into a simple, one-dimensional descriptor that provides a good prediction of T_0 in these alloys.

*tanmoy.chakraborty@rub.de

The paper is organized as follows: In Sec. II, we summarize the computational details. In Sec. III, a description of the structure of the involved phases is given. Section IV comprises the methodology that we use to compute the different contributions to the free energy of the phases. We discuss our main results in combination with available experimental findings in Sec. V. We propose a new parameter in Sec. VI for the further development of HTSMAs in particular in computationally guided high-throughput research and summarize our findings in Sec. VII.

II. COMPUTATIONAL DETAILS

Density functional theory (DFT) calculations were carried out using the projector augmented wave (PAW) [25] method as implemented in the Vienna *ab initio* simulation package (VASP) [26–28]. The PAW potentials include $3p$ and $5p$ electrons in the valence shell for Ti and Ta, respectively. The Perdew-Burke-Ernzerhof parametrization of the generalized gradient approximation was used for the exchange-correlation functional (PBE-GGA) [29]. The calculations were performed with an energy cutoff of 300 eV for the plane waves and the Methfessel-Paxton scheme was used to integrate the Brillouin zone (BZ) with a smearing of $\sigma = 0.05$ eV. Within our computational setup total energies were converged to within 4 meV/atom. Structures were relaxed until all forces were below 10^{-3} eV/Å. Single-crystal elastic constants were obtained from the stress-strain relationship using the symmetry-general least-squares extraction method proposed by Le Page and Saxe [30] as implemented in VASP. The Monkhorst-Pack [31] scheme was used to distribute the k points in the reciprocal space.

III. THE MARTENSITE AND AUSTENITE PHASE IN Ti-Ta

Within our study we consider five compositions of Ti-Ta alloys, namely, Ti with 12.5%, 18.75%, 25%, 31.25%, and 37.5% Ta. For each composition we fully optimize the lattice vectors and internal coordinates. To represent the chemical disorder in the Ti-Ta alloys, we use the special quasirandom structure (SQS) method [32] as implemented in the modified version [33,34] of the ATAT package [35].

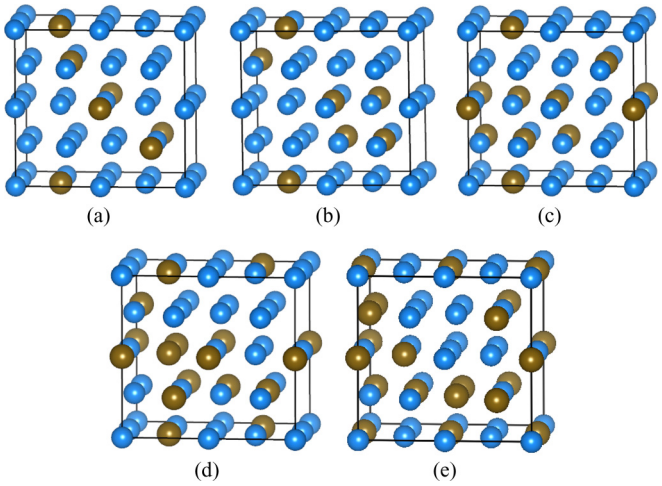

FIG. 1. SQSs of the α'' phase for different Ta content. Light blue and gold atoms represent the Ti and Ta atoms, respectively.(a) $Ti_{28}Ta_4$; (b) $Ti_{26}Ta_6$; (c) $Ti_{24}Ta_8$; (d) $Ti_{22}Ta_{10}$; (e) $Ti_{20}Ta_{12}$.

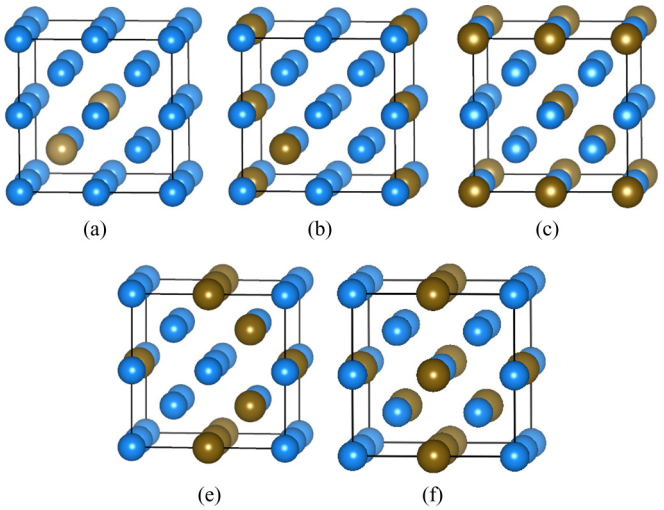

FIG. 2. SQSs of the β phase for different Ta content. Light blue and gold atoms represent the Ti and Ta atoms, respectively. (a) $Ti_{14}Ta_2$; (b) $Ti_{13}Ta_3$; (c) $Ti_{12}Ta_4$; (d) $Ti_{11}Ta_5$; (e) $Ti_{10}Ta_6$.

The equilibrium lattice vectors of the orthorhombic α'' phase (low-temperature martensite) were obtained by fitting the energy versus volume curves with the Murnaghan equation of state [36,37] where for each volume the b/a and c/a ratios were optimized. The Wyckoff positions of the atoms in the α'' phase are given by (0,0,0), (1/2,1/2,0), $(0,1-2y,1/2)$, and $(1/2,1/2-2y,1/2)$, with $y \approx 0.2$. The y value was fully relaxed for all structures. For all compositions, $(2 \times 2 \times 2)$ supercells containing 32 atoms were used with $[7 \times 6 \times 6]$ Monkhorst-Pack [31] k-point meshes. The values of the correlation function for the corresponding SQSs were 0.0165, 0.0105, 0.0045, 0.0044, and 0.0045 for 12.5%, 18.75%, 25%, 31.25%, and 37.5% Ta, respectively. The SQS supercells of the α'' phase for different Ta contents are shown in Fig. 1. The optimized lattice vectors are compiled in Table I. With increasing Ta content, the volume/atom of the α'' phase increases which is consistent with previous theoretical and experimental studies [38–43].

The β phase (high-temperature austenite) has a body-centered-cubic (bcc) structure. For all compositions, we used $(2 \times 2 \times 2)$ supercells containing 16 atoms with $[12 \times 12 \times 12]$ Monkhorst-pack k-point meshes. Atomic positions were fully relaxed. The lattice vectors of the β phase were optimized by fitting the energy-volume curves with Murnaghan's equation of state. The correlation function values of the SQSs in this case were 0.0722, 0.0439, 0.0236, 0.0121, and 0.008, respectively. The supercells of the SQS of the β phase for different Ta content are shown in Fig. 2. In Table I, the optimized lattice constants of the β phase are compiled. We find a similar trend of the volume/atom with composition as in the α'' phase, however, the absolute volume/atom differs between the two phases at the same composition. The composition dependence of the lattice constant of the β phase is in good agreement with previous studies [38–43].

TABLE I. Optimized lattice parameters a_0, b_0, and c_0 (in Å), ratio of lattice parameters, and volume/atom Ω_0 (in Å^3) of the α'' and β phases for different Ta content.

	Martensite (α'')						Austenite (β)	
Composition	a_0	b_0	c_0	b_0/a_0	c_0/a_0	Ω_0	a_0	Ω_0
Ti-12.5Ta	3.083	4.948	4.587	1.605	1.488	17.49	3.260	17.32
Ti-18.75Ta	3.232	4.861	4.463	1.504	1.381	17.53	3.263	17.37
Ti-25Ta	3.310	4.767	4.454	1.440	1.345	17.57	3.265	17.40
Ti-31.25Ta	3.333	4.750	4.452	1.425	1.335	17.62	3.270	17.48
Ti-37.5Ta	3.343	4.721	4.485	1.412	1.341	17.69	3.274	17.55

IV. FREE-ENERGY CONTRIBUTIONS

The martensitic transformation is a diffusionless first-order transformation where it is assumed that the composition is identical in the two phases. We therefore compare the free energies of the martensite and austenite phases in Ti-Ta at the same composition to obtain the transformation temperature. In order to access the free energy at finite temperatures, we apply an adiabatic approach to evaluate the different contributions separately:

$$F(V,T) = E(V) + F_{\mathrm{el}}(V,T) - T S_{\mathrm{mix}} + F_{\mathrm{vib}}(V,T), \quad (1)$$

where $E(V)$ is the $T = 0$ K total energy, $F_{\mathrm{el}}(V,T)$ the electronic contribution, S_{mix} the configurational entropy, and $F_{\mathrm{vib}}(V,T)$ the vibrational contribution.

The 0-K total energies are directly obtained from our DFT calculations. The electronic contribution to the free energy $F_{\mathrm{el}}(V,T)$ is extracted from the DFT calculations based on the Fermi-Dirac smearing [44]. We apply an appropriate smearing width σ to obtain the total energy for a particular temperature T using $\sigma = k_{\mathrm{B}}T$. The total energy is then subtracted from $\sigma = 0$ (i.e., $T = 0$) calculations to get the electronic entropy at T.

The configurational entropy of a binary solid solution can be approximated within the ideal mixing approach $S_{\mathrm{mix}} = -k_{\mathrm{B}}[x \ln x + (1-x)\ln(1-x)]$ where x is the fraction of one of the components. Within this approach, the contribution to the free energy is constant for a particular composition and the configurational entropy term cancels out when calculating free-energy differences between phases with the same chemical composition.

A commonly used approach to obtain the vibrational free energy $F_{\mathrm{vib}}(V,T)$ is based on the phonon density of states (DOS) [45]. This is not applicable if the considered phase is dynamically unstable at $T = 0$ K as reflected by imaginary phonon frequencies. In this case, finite-temperature techniques need to be considered including, e.g., self-consistent *ab initio* lattice dynamics (SCAILD) [46] or molecular dynamics (MD) simulations [47]. These approaches are computationally very demanding, in particular for systems with low crystal symmetry. In Ti-Ta alloys, the high-temperature austenite phase is dynamically unstable for low Ta concentrations at $T = 0$ K exhibiting imaginary phonon branches throughout the entire Brillouin zone [43]. We have verified this for our SQS supercells where these structures produce a large number of displacements owing to their low crystal symmetry, making phonon calculations computationally very expensive.

In this study, we use the quasiharmonic Debye model [48] to calculate the vibrational free energy as implemented in the GIBBS code [49]. The quasiharmonic Debye model has been applied successfully to several systems [50–53] including pure Ti [54,55], where the reported results compare well to results from the other methods discussed above. Although the free energies obtained within the Debye model might not be highly accurate, we can obtain reliable trends as a function of composition within this computationally efficient approach. Within the Debye model [56], the vibrational free energy is given by

$$F_{\mathrm{vib}}[\Theta_{\mathrm{D}}(V),T] = n k_{\mathrm{B}} T \left[\frac{9}{8}\frac{\Theta_{\mathrm{D}}(V)}{T} + 3\ln(1 - e^{-\Theta_{\mathrm{D}}(V)/T}) - D[\Theta_{\mathrm{D}}(V)/T] \right], \quad (2)$$

where $\frac{9}{8}k_{\mathrm{B}}\Theta_{\mathrm{D}}$ is the zero-point vibrational energy, k_{B} is the Boltzmann constant, V is the volume, T is the temperature, and n is the number of atoms per formula unit. $D(\frac{\Theta_{\mathrm{D}}}{T})$ is the Debye function given by

$$D(\Theta_{\mathrm{D}}/T) = 3\left(\frac{T}{\Theta_{\mathrm{D}}}\right)^3 \int_0^{\Theta_{\mathrm{D}}/T} \frac{x^3}{e^x - 1} dx. \quad (3)$$

Θ_{D} is the Debye temperature which for an isotropic solid can be calculated from

$$\Theta_{\mathrm{D}} = \frac{\hbar}{k_{\mathrm{B}}}[6\pi^2 V^{1/2} n]^{1/3} f(\nu)\sqrt{\frac{B_S}{M}}, \quad (4)$$

where $\hbar$ is the reduced Planck constant, M is the molecular mass per unit formula, and B_S is the adiabatic bulk modulus which is assumed as static compressibility and further simplified in this model [49]

$$B_S \cong B(V) = V\frac{d^2E(V)}{dV^2}. \quad (5)$$

The function $f(\nu)$ of the Poisson ratio ν is given by

$$f(\nu) = \left\{ 3\left[2\left(\frac{2}{3}\frac{1+\nu}{1-2\nu}\right)^{3/2} + \left(\frac{1}{3}\frac{1+\nu}{1-\nu}\right)^{3/2} \right]^{-1} \right\}^{1/3}. \quad (6)$$

In the quasiharmonic Debye model, Θ_{D} is a function of the volume which changes with temperature. The approximation to $\Theta_{\mathrm{D}}(V)$ given in Eq. (4) was suggested by Slater [57], where the calculation of transversal and longitudinal sound velocities is replaced by elastic constants. It is thus important to obtain reliable values of the elastic constants for the investigated structures.

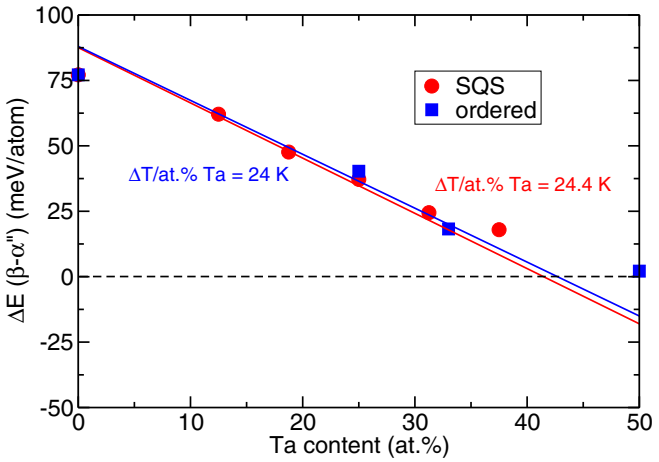

FIG. 3. 0-K energy difference between austenite and martensite as a function of Ta content. Blue squares represent the ordered structures taken from our previous work [43], red circles represent the disordered SQSs used in this work.

Although we find in our previous work [43] that the austenite structures exhibit imaginary phonon frequencies, the calculated elastic constants in this study still fulfill the elastic stability criteria [58] and all eigenvalues of the elastic tensor matrix are positive, which allows us to obtain a reasonable estimate of the Poisson ratio ν. The imaginary phonon frequencies belong to both optical and short-wavelength acoustic branches, whereas the elastic constants originate from the long-wavelength acoustic phonon branches, and we do not observe any imaginary acoustic branches near the Γ point in the phonon DOS. We also obtain a good description of the mechanical compressibility B_S.

To calculate the Poisson ratio ν for the anisotropic Ti-Ta alloys, we use the average bulk and shear modulus of the Voigt and Reuss bounds for polycrystalline materials [59–61]

$$\nu = \frac{3B - 2G}{2(3B + G)}, \tag{7}$$

where B and G are the average bulk and shear modulus

$$B = \tfrac{1}{2}(B_V + B_R) \tag{8}$$

and

$$G = \tfrac{1}{2}(G_V + G_R), \tag{9}$$

and B_V, B_R, G_V, and G_R are the bulk and shear modulus from the Voigt and Reuss equations, respectively. The relation between the bulk and shear modulus and the elastic constants is discussed in Appendix A.

V. COMPOSITION-DEPENDENT TRANSFORMATION TEMPERATURE

A. Total-energy difference

The first contribution to the free energy in Eq. (1) is the total energy. As we are interested in the free-energy differences between the austenite (β) and martensite (α'') phases, we show in Fig. 3 the 0-K total-energy difference $\Delta E = E(\beta) - E(\alpha'')$ as a function of Ta content. The positive-energy difference implies that the martensite is energetically more favorable than the austenite within the studied composition range. The energy difference decreases with increasing Ta content. The linear fit of the data points yields a slope of ~ -2 meV/atom at. % which translates to ~24 K at. % Ta.

We also compare the results from the SQS supercells with our previous study (blue squares in Fig. 3) where we considered chemically ordered structures [43]. There is no significant difference between the results from the chemically ordered and disordered structures which is due to the small ordering energy in Ti-Ta alloys. The linear dependence of the energy difference on the composition can be rationalized within a simple d-band model [62] where with the increase in Ta content the number of electrons in the Ti-Ta alloy increases, which in turn stabilizes the bcc structure of the β phase (austenite). Thus, the filling of the d band leads to a gradual change in relative phase stability. The calculated phase stability at 0 K between the martensite and the austenite is in good agreement with experimental findings [41,42].

The behavior of the relative phase stabilities in Ti-Ta alloys differs significantly from Ni-Ti based SMAs. The main difference occurs due to their structural arrangements. Ti-Ta is a disordered alloy whereas Ni-Ti exhibits an ordered structure. In the ordered Ni-Ti phases, the formation energy difference is strongly influenced by the local relaxations around antisite defects [24]. The energy difference between the B2 (austenite) and B19′ (martensite) phases remains roughly constant up to an equiatomic composition, then a sharp drop in the energy difference is observed which is a consequence of stabilization of the B2 phase by the structural relaxations around Ni antisite atoms.

B. Vibrational free energy

The Debye temperature depends mainly on the Poisson's ratio ν and thus a reliable estimate of ν is necessary for a good description of the vibrational entropy contribution. Since the Voigt and Reuss approximations are based on uniform strain and stress, respectively, applied on an aggregate, any measured moduli should lie between these limits. The upper and lower limits of ν for α'' and β as a function composition are compiled in Table II. At low Ta content, the upper and lower bounds of ν differ significantly for both phases. This is clearly a consequence of the highly anisotropic nature of the phases at low Ta content. With increasing Ta concentration, the difference between the upper and lower limits of ν decreases for both phases, indicating a decrease in anisotropy. The variation of ν as a function of composition is shown in Fig. 4. The black and red symbols indicate the Poisson ratio of the martensite and austenite, respectively. The ν values of the two phases show a different dependence on the composition: for the martensite ν initially decreases, reaches a minimum value at 25% Ta, and then increases with further addition of Ta. For the austenite ν monotonically decreases over the entire composition range.

The behavior of ν as a function composition is inverse to the corresponding Debye temperature compiled in Table II. In Fig. 5, we plot the Debye temperature (Θ_D) of both phases and their difference ($\Delta\Theta$) at 0 K as a function of composition. Both phases have a similar Θ_D at low and high Ta concentrations

TABLE II. Calculated Voigt (ν_V), Reuss (ν_R), and the average Poisson's ratio (ν_H) of the martensite and austenite as a function of composition. The corresponding Debye temperature (Θ_D) is also shown.

	Martensite (α'')				Austenite (β)			
Composition	ν_V	ν_R	ν_H	Θ_D	ν_V	ν_R	ν_H	Θ_D
Ti-12.5Ta	0.380	0.478	0.429	224	0.399	0.497	0.448	189
Ti-18.75Ta	0.352	0.417	0.384	271	0.397	0.457	0.427	215
Ti-25Ta	0.341	0.372	0.356	291	0.393	0.438	0.415	224
Ti-31.25Ta	0.342	0.365	0.353	284	0.386	0.414	0.400	240
Ti-37.5Ta	0.349	0.366	0.357	273	0.384	0.404	0.394	241

but with increasing Ta content Θ_D of the austenite increases approximately linearly over the entire composition range, whereas for the martensite it reaches a maximum at 25% Ta and then starts to decrease again. The strong correlation between ν and Θ_D indicates that the Poisson ratio is central to the Debye temperature which in turn determines the vibrational entropy of the two phases.

C. Free-energy calculations

In Fig. 6, we show the free-energy difference $\Delta F = F_\beta - F_{\alpha''}$ for five different compositions. For $\Delta F > 0$ the α'' phase (martensite) is more stable and for $\Delta F < 0$ the β phase (austenite). At low temperatures, the martensite is the stable phase for all compositions and the transition temperature T_0 is extracted from $\Delta F = 0$. The red lines in Fig. 6 describe the total free-energy difference (ΔF), black lines indicate the difference in vibrational free energy (ΔF_{vib}), and the green lines depict the difference in electronic free energy (ΔF_{el}) between austenite and martensite. The value of ΔF_{vib} at $T = 0$ K has a minimum at about 25% and also the slope of the ΔF_{vib} curves is different for the five compositions. This is mainly due to the difference in the Debye temperature between the phases ($\Delta\Theta$) which has a maximum at 25% Ta content as discussed in Sec. V B. The difference in the electronic free-energy contribution ΔF_{el} does not change much with composition. As the overall difference increases with increasing temperature the electronic contribution changes T_0 significantly for large transition temperatures. For 12.5% Ta content, T_0 is overestimated by ~170 K (~ 15%) if ΔF_{el} is not taken into account. For 25% Ta, on the other hand, ΔF_{el} changes T_0 only by ~30 K (~ 6%). The total free-energy difference ΔF at $T = 0$ K decreases more quickly up to 25% Ta and continues to decrease relatively slowly for higher Ta concentrations. The transition temperature T_0 decreases with the addition of Ta over the entire composition range which is in agreement with experimental findings [2].

In Fig. 7, the predicted transition temperatures T_0 (blue squares) are compared to experimentally measured values of M_s (red circles) [63]. With increasing Ta content, the calculated T_0 values initially decrease linearly, showing a strong composition dependence. The effect of additional Ta alloying becomes weaker for higher concentrations and T_0 seems to become almost independent of the composition. Within a composition range of 17% $\leqslant$ Ta $\leqslant$ 32% the absolute values as well as the trend in T_0 compare very well to the experimentally measured M_s. For high and low Ta concentrations there are, however, some deviations. There are several possible reasons for the observed discrepancies, including the limitations of the Debye model, an accurate description of the two phases within the employed supercells, as well as the occurrence of mixed phases in the experiments. At very low Ta content (12.5%), it is unlikely to observe a

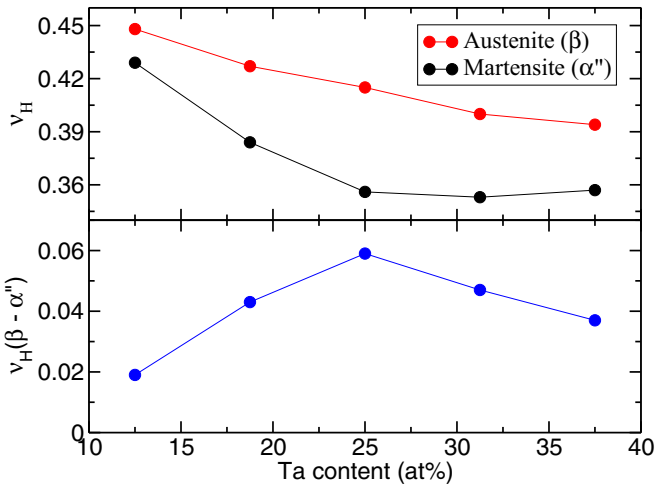

FIG. 4. 0-K Poisson's ratio of the martensite (black) and the austenite (red) as a function of Ta content (upper panel) and their difference (lower panel).

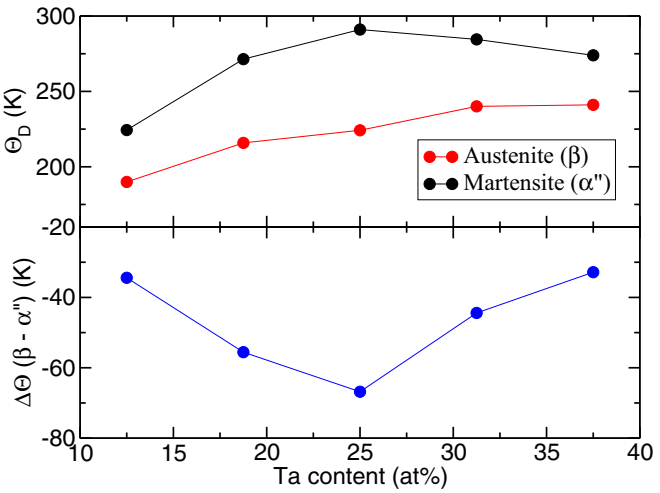

FIG. 5. 0-K Debye temperature of the martensite (black) and the austenite (red) (upper panel) and difference (lower panel).

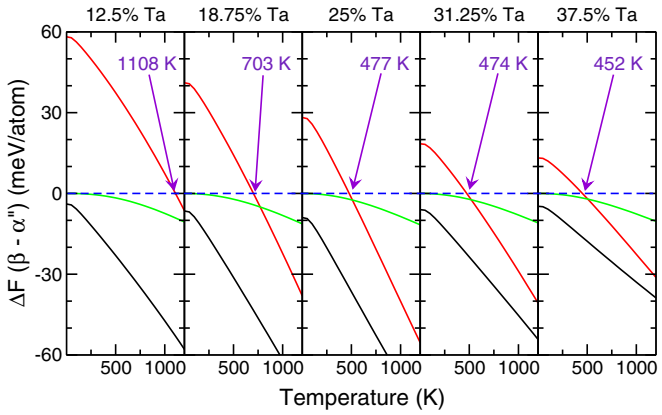

FIG. 6. Calculated free-energy difference between austenite and martensite as a function of alloying element. The red, black, and the green lines indicate the difference of total, vibrational, and the electronic free energies between the phases, respectively.

stable martensitic transformation as the detrimental ω phase is likely to form [43]. Also, the Debye temperatures of the two phases are very similar at this composition which together with a large total energy-difference at $T = 0$ K leads to a very high transformation temperature. At high concentrations of 36% and 40% Ta, a mixture of the α'' and β phases was observed experimentally [2], whereas within our calculations we consider single-phase materials. A direct comparison of the measured M_s with the calculated T_0 might therefore not be applicable for these compositions. In addition, we assume both phases to be at least metastable at $T = 0$ K for all compositions. Despite the discussed deviations between the experimental and theoretical results, the overall agreement in the trend as well as the absolute values of T_0 and M_s as shown in Fig. 7 is remarkable considering the approximations underlying our approach.

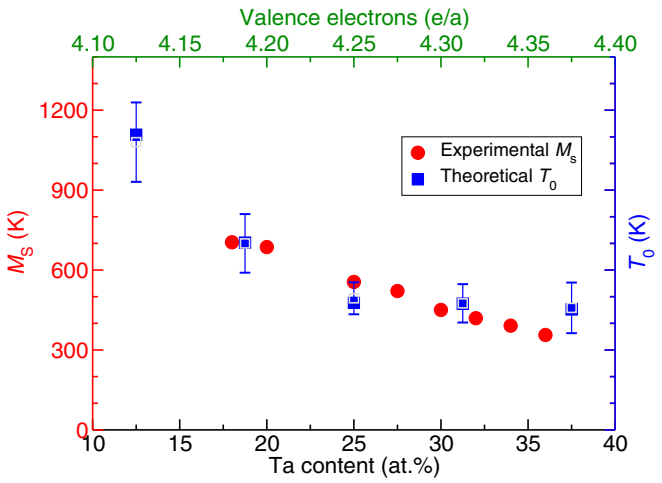

FIG. 7. Calculated transition temperatures between austenite and martensite (blue squares) and compared with experiments [63] (red circles). The open squares and the error bars represent the mean value and standard deviation over 100 calculations by randomly varying the elastic constants of one phase by ±10% and the difference in elastic constants between the two phases by ±3%.

The largest uncertainty in the transition temperature arises due to the inaccuracy in the calculation of elastic constants. To estimate the corresponding error in T_0 we have randomly varied the elastic constants of one phase within an interval of ±10% and the difference in elastic constants between the two phases by ±3%. For each composition, 100 transition temperatures were calculated within the interval including also the electronic entropy contributions. The mean values and corresponding standard deviation are shown as open squares and error bars in Fig. 7.

In the upper x axis of Fig. 7 we also show the number of valence electrons per atom (e/a) at each composition. As the e/a ratio increases linearly with increasing Ta content, T_0 decreases with increasing valence electron number. This analysis is again different from the binary Ni-Ti system where instead of the e/a ratio the structural stabilization of the austenite determines the composition dependence of M_s [24].

Similar *ab initio* approaches have recently been applied to determine the phase stability in binary Ti-Ta alloys including a phase diagram [64,65]. Huang *et al.* [64] compared the calculated phase boundaries with experimental M_s [2] and found a much worse agreement with experiment than we observe in Fig. 7. The reason for this is that they only considered the transition between the β and α/ω phases, whereas the martensitic transformation in Ti-Ta HTSMAs is between the β and α'' phases as discussed in this work.

VI. A SIMPLE APPROXIMATION TO M_s

The total-energy difference ΔE and the difference in vibrational free energy ΔF_{vib} are the main contributions to ΔF. To simplify, we therefore approximate the total free-energy difference between the phases as

$$\Delta F \approx \Delta E + \Delta F_{\text{vib}} = [E_\beta - E_{\alpha''}] + [F_{\text{vib}}(\Theta_{\text{D}}^{\beta}) - F_{\text{vib}}(\Theta_{\text{D}}^{\alpha''})], \quad (10)$$

where E_β and $E_{\alpha''}$ are the $T = 0$ K total energies and Θ_β and $\Theta_{\alpha''}$ are the Debye temperatures of the austenite (β) and martensite (α''), respectively. We have evaluated Eq. (10) analytically within the harmonic approximation for different values of ΔE and $\Delta\Theta = \Theta_\beta - \Theta_{\alpha''}$ and determined T_0 from $\Delta F = 0$. The corresponding plot of T_0 as a function of ΔE and $\Delta\Theta$ is shown in Fig. 8. The red line in Fig. 8 indicates a value of $T_0 = 373$ K above which ideal candidates for HTSMA can be found, i.e., the contour plot can be used as a map to quickly evaluate transition temperatures of alloys. Since the α'' phase is stable at low temperatures and the β phase needs to become stable at high temperatures, we require $\Delta E > 0$ and $\Delta\Theta < 0$ to observe a crossing of the free-energy curves. Figure 8 shows that T_0 is proportional to ΔE and $1/\Delta\Theta$, i.e., T_0 increases as the difference in E increases and the difference in Θ decreases between the two phases, respectively.

It is straightforward to show that in the high-temperature limit a linear dependence of T_0 on ΔE and $1/\Delta\Theta$ is obtained:

$$T_0 \propto -\frac{\Delta E}{\Delta\Theta} = \frac{U}{\Theta_{\text{D}}}. \quad (11)$$

A derivation of this relationship is given in Appendix B.

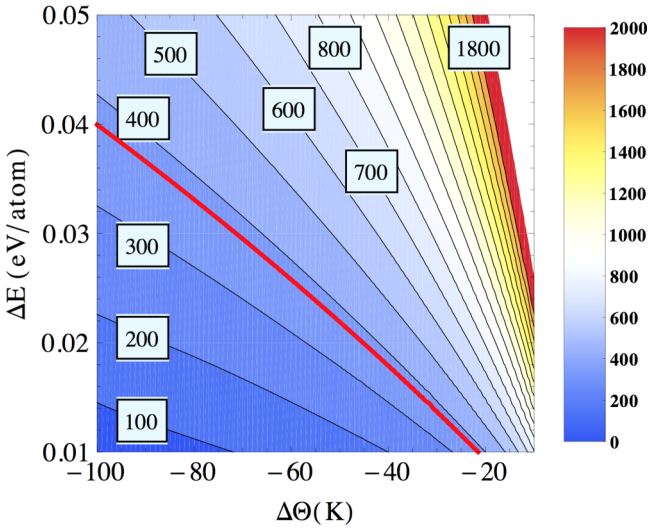

FIG. 8. Transition temperature T_0 as a function of ΔE and $\Delta\Theta$.

In Fig. 9, the values extracted from Fig. 8 are shown in a one-dimensional plot. The black circles in Fig. 9 are the average values of the slope from the ΔE versus $\Delta\Theta$ curve for a particular temperature. The error bars represent the deviation of T_0 from a perfect linear behavior. The error bars increase with increasing of T_0, implying that the simple harmonic approximation strictly only holds for low temperatures. The red circles in Fig. 9 are the values of T_0 taken from Fig. 7 which are calculated within the quasiharmonic approximation, i.e., $\Delta\Theta$ depends on the volume and therefore on T. It can be seen that our simple analytic model works well for low temperatures, but for higher values of T_0 there are larger deviations. This is due to the fact that at higher temperatures the electronic contributions play a more significant role as well as quasiharmonic effects. It follows from Eq. (11) that the larger ΔE and the smaller $\Delta\Theta$ the larger is T_0 and vice versa, which again nicely explains our results shown in Fig. 7. In Ti-Ta alloys, ΔE decreases (Fig. 3) and $\Delta\Theta$ increases (Fig. 5) for low Ta concentrations and therefore T_0 strongly decreases. For higher concentrations, however, starting from 25% Ta both

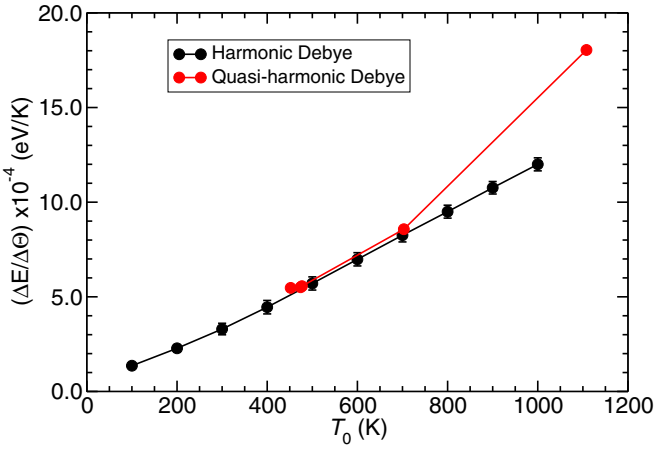

FIG. 9. Parameter $\Delta E/\Delta\Theta$ as a function of transition temperature T_0 for harmonic and quasiharmonic Debye models.

ΔE and $\Delta\Theta$ decrease in a similar fashion, so that T_0 is almost constant.

Overall, the agreement of our simple model with the experimentally observed composition dependence of martensitic transformation temperatures is remarkable. We conclude that the total-energy difference as well as the difference in elastic properties (and thus in the Debye temperature) are indeed the two critical parameters that control the transformation temperature in this alloy system. The ratio $\Delta E/\Delta\Theta$ can therefore serve as a simple, one-dimensional descriptor to estimate T_0 (and therefore M_s), e.g., in high-throughput screening of ternary or multicomponent alloys for the further development of HTSMAs. To obtain an alloy with a high transformation temperature, there should be a large difference in the phase stability between the martensite and austenite at $T = 0$ K, and the difference in the Debye temperature via the elastic properties between the two phases should be as small as possible.

VII. CONCLUSION

We have used DFT calculations in combination with the quasiharmonic Debye model to unravel the strong composition dependence of the martensitic start temperature M_s in Ti-Ta high-temperature shape memory alloys. Within this special class of materials systems we find that there are two physical key parameters that determine the transformation temperature: (a) the relative phase stability of the martensite and austenite at $T = 0$ K and (b) the difference in the elastic properties of the two phases that directly influence the vibrational contribution to the free energy. From the analysis of our computational results, we identify a simple, one-dimensional descriptor that may be used to estimate M_s in high-throughput screening of ternary or multicomponent alloys for a computationally guided development of high-temperature shape memory alloys.

ACKNOWLEDGMENTS

This work is financially supported by Deutsche Forschungsgemeinschaft (DFG) within TP3 of the research unit FOR 1766 (High Temperature Shape memory alloys, see: http://www.for1766.de).

APPENDIX A: RELATIONSHIP BETWEEN SINGLE-CRYSTAL ELASTIC CONSTANTS AND POLYCRYSTALLINE PROPERTIES

The full elastic tensor matrix for an orthorhombic crystal structure is given by

$$\begin{pmatrix} C_{11} & C_{12} & C_{13} & 0 & 0 & 0 \\ C_{12} & C_{22} & C_{23} & 0 & 0 & 0 \\ C_{13} & C_{22} & C_{33} & 0 & 0 & 0 \\ 0 & 0 & 0 & C_{44} & 0 & 0 \\ 0 & 0 & 0 & 0 & C_{55} & 0 \\ 0 & 0 & 0 & 0 & 0 & C_{66} \end{pmatrix}.$$

For a cubic crystal, $C_{11} = C_{22} = C_{33}$, $C_{12} = C_{13} = C_{23}$, and $C_{44} = C_{55} = C_{66}$. Using special quasirandom structures to describe the disordered β phase results in a lowering of the

symmetry and slight differences in the elastic constants that are equivalent in the cubic phase. To obtain the values for the cubic structures, we have averaged the corresponding elastic constants as follows:

$$\begin{aligned}\overline{C_{11}} &= (C_{11}+C_{22}+C_{33})/3,\\ \overline{C_{12}} &= (C_{12}+C_{13}+C_{23})/3,\\ \overline{C_{44}} &= (C_{44}+C_{55}+C_{66})/3.\end{aligned} \tag{A1}$$

The relationship between the single-crystal elastic constants and their inverse matrix elements with the polycrystalline bulk and shear moduli are discussed [66,67] and recalled here:

(i) Cubic phase:

$$B_V = B_R = (C_{11}+2C_{12})/3, \tag{A2}$$

$$G_V = (C_{11}-C_{12}+3C_{44})/5, \tag{A3}$$

$$G_R = 5(C_{11}-C_{12})C_{44}/[4C_{44}+3(C_{11}-C_{12})]. \tag{A4}$$

(ii) Orthorhombic phase:

$$B_V = \tfrac{1}{9}(C_{11}+C_{22}+C_{33}) + \tfrac{2}{9}(C_{12}+C_{23}+C_{13}), \tag{A5}$$

$$G_V = \tfrac{1}{15}[C_{11}+C_{22}+C_{33}-(C_{12}+C_{23}+C_{13})] + \tfrac{1}{5}(C_{44}+C_{55}+C_{66}), \tag{A6}$$

$$\frac{1}{B_R} = (S_{11}+S_{22}+S_{33}) + 2(S_{12}+S_{13}+S_{23}), \tag{A7}$$

$$\frac{1}{G_R} = \frac{1}{15}[4(S_{11}+S_{22}+S_{33}) - (S_{12}+S_{13}+S_{23}) + 3(S_{44}+S_{55}+S_{66})], \tag{A8}$$

where S_{11}, S_{12}, etc., are the elastic compliance matrix elements and can be obtained from the mathematical relationship between the matrix stiffness C_{ij} and the compliance coefficients S_{ij}.

APPENDIX B: RELATIONSHIP BETWEEN ΔE, $\Delta\Theta$, AND T_0

We choose an expansion parameter $\Theta_D = \frac{1}{2}[\Theta_D^{\beta} + \Theta_D^{\alpha''}]$; $\Delta\Theta = [\Theta_D^{\beta} - \Theta_D^{\alpha''}]$. Assuming $\Theta_D \gg \Delta\Theta$ and expanding $F_{\rm vib}(\Theta)$ in a Taylor series around Θ_D we obtain

$$F_{\rm vib}(\Theta_D \pm \Delta\Theta) = F_{\rm vib}(\Theta_D) \pm F'(\Theta_D)\Delta\Theta + \tfrac{1}{2}F''(\Theta_D)\Delta\Theta^2 + \dots. \tag{B1}$$

For the free energies of the two phases we correspondingly obtain

$$\begin{aligned}F_{\rm vib}\left(\Theta_D^{\beta}\right) &= F_{\rm vib}(\Theta_D) + \tfrac{1}{2}F'(\Theta_D)\Delta\Theta + \dots,\\ F_{\rm vib}\left(\Theta_D^{\alpha''}\right) &= F_{\rm vib}(\Theta_D) - \tfrac{1}{2}F'(\Theta_D)\Delta\Theta + \dots,\end{aligned} \tag{B2}$$

and, thus,

$$\Delta F_{\rm vib} = F_{\rm vib}\left(\Theta_D^{\beta}\right) - F_{\rm vib}\left(\Theta_D^{\alpha''}\right) \approx F'(\Theta_D)\Delta\Theta. \tag{B3}$$

At the transition temperature T_0, $\Delta F = 0$ which yields

$$\Delta E + F'(\Theta_D)\Delta\Theta = 0. \tag{B4}$$

Both ΔE and $\Delta\Theta$ are treated within the harmonic approximation and considered to be temperature independent.

For the Debye model in Eq. (2), it is straightforward to show that

$$\frac{dF}{d\Theta_D} = \frac{U}{\Theta_D}, \tag{B5}$$

where U is the internal energy of the system. Therefore, from Eq. (B4) we expect

$$-\frac{\Delta E}{\Delta\Theta} \approx \frac{dF}{d\Theta_D} = \frac{U}{\Theta_D}. \tag{B6}$$

As $U - U_0 = 3Nk_BT$ in the high-temperature limit, we expect $\Delta E/\Delta\Theta$ to be a linear function of T above Θ_D.

[1] J. Ma, I. Karaman, and R. Noebe, Int. Mater. Rev. **55**, 257 (2010).
[2] P. J. S. Buenconsejo, H. Y. Kim, H. Hosoda, and S. Miyazaki, Acta Mater. **57**, 1068 (2009).
[3] G. S. Firstov, J. V. Humbeeck, and Y. N. Koval, Mater. Sci. Eng., A **378**, 2 (2004).
[4] M. Ikeda, S. Y. Komatsu, and Y. Nakamura, Mater. Trans. **45**, 1106 (2004).
[5] D. H. Ping, Y. Mitarai, and F. X. Yin, Scr. Mater. **52**, 1287 (2005).
[6] C. Baker, Met. Sci. J. **5**, 92 (1971).
[7] P. J. S. Buenconsejo, H. Y. Kim, and S. Miyazaki, Scr. Mater. **64**, 1114 (2011).
[8] B. S. Hickman, J. Mater. Sci. **4**, 554 (1969).
[9] D. de Fontaine, Acta. Metall. **18**, 275 (1970).
[10] H. Y. Kim, S. Hashimoto, J. I. Kim, T. Inamura, H. Hosoda, and S. Miyazaki, Mater. Sci. Eng., A **417**, 120 (2006).
[11] H. Y. Kim, Y. Ikehara, J. I. Kim, H. Hosoda, and S. Miyazaki, Acta Mater. **54**, 2419 (2006).
[12] P. J. S. Buenconsejo, H. Y. Kim, and S. Miyazaki, Acta Mater. **57**, 2509 (2009).
[13] F. Falk, Acta. Metall. **28**, 1773 (1980).
[14] F. Falk and J. Konopka, J. Phys.: Condens. Matter **2**, 61 (1990).
[15] O. Nittono and Y. Koyama, Jpn. J. Appl. Phys. **21**, 680 (1982).
[16] J. K. Liakos and G. A. Saunders, Philos. Mag. A **46**, 217 (1982).
[17] G. R. Barsch and J. A. Krumhansl, Phys. Rev. Lett. **53**, 1069 (1984).

[18] X. B. Ren and K. Otsuka, Mater. Sci. Forum **327**, 429 (2000).
[19] J.-M. Lu, Q.-M. Hu, and R. Yang, Acta Mater. **56**, 4913 (2008).
[20] X. Ren, N. Miura, J. Zhang, K. Otsuka, K. Tanaka, M. Koiwa, T. Suzuki, Y. I. Chumlyakov, and M. Asai, Mater. Sci. Eng., A **312**, 196 (2001).
[21] M. Zarinejad and Y. Liu, Adv. Funct. Mater. **18**, 2789 (2008).
[22] K. Otsuka and X. Ren, Prog. Mater. Sci. **50**, 511 (2005).
[23] X. Ren, K. Taniwaki, K. Otsuka, T. Suzuki, K. Tanaki, Y. I. Chumlyakov, and T. Ueiki, Philos. Mag. A **79**, 31 (1999).
[24] J. Frenzel, A. Wieczorek, I. Opahle, B. Maaß, R. Drautz, and G. Eggeler, Acta Mater. **90**, 213 (2015).
[25] P. E. Blöchl, Phys. Rev. B **50**, 17953 (1994).
[26] G. Kresse and J. Furthmüller, Comput. Mater. Sci. **6**, 15 (1996).
[27] G. Kresse and J. Furthmüller, Phys. Rev. B **54**, 11169 (1996).
[28] G. Kresse and D. Joubert, Phys. Rev. B **59**, 1758 (1999).
[29] J. P. Perdew, K. Burke, and M. Ernzerhof, Phys. Rev. Lett. **77**, 3865 (1996).
[30] Y. LePage and P. Saxe, Phys. Rev. B **65**, 104104 (2002).
[31] H. J. Monkhorst and J. D. Pack, Phys. Rev. B **13**, 5188 (1976).
[32] A. Zunger, S. H. Wei, L. G. Ferreira, and J. E. Bernard, Phys. Rev. Lett. **65**, 353 (1990).
[33] J. von Pezold, A. Dick, M. Friák, and J. Neugebauer, Phys. Rev. B **81**, 094203 (2010).
[34] J. Koßmann, T. Hammerschmidt, S. Maisel, S. Müller, and R. Drautz, Intermetallics **64**, 44 (2015).
[35] A. van de Walle, M. Asta, and G. Ceder, CALPHAD: Comput. Coupling Phase Diagrams Thermochem. **26**, 539 (2002).
[36] F. Birch, J. Appl. Phys. **9**, 279 (1938).
[37] F. Birch, Phys. Rev. **71**, 809 (1947).
[38] H. Ikehata, N. Nagasako, T. Furuta, A. Fukumoto, K. Miwa, and T. Saito, Phys. Rev. B **70**, 174113 (2004).
[39] C. Y. Wu, Y. H. Xin, X. F. Wang, and J. G. Lin, Solid State Sci. **12**, 2120 (2010).
[40] C. X. Li, H. B. Luo, Q. M. Hu, R. Yang, F. X. Yin, O. Umezawa, and L. Vitos, Solid State Commun. **159**, 70 (2013).
[41] A. V. Dobromyslov and V. A. Elkin, Scr. Mater. **44**, 905 (2001).
[42] A. V. Dobromyslov and V. A. Elkin, Mater. Sci. Eng. A **438**, 324 (2006).
[43] T. Chakraborty, J. Rogal, and R. Drautz, J. Phys.: Condens. Matter **27**, 115401 (2015).
[44] N. D. Mermin, Phys. Rev. **137**, A1441 (1965).
[45] W. Cochran and R. A. Cowley, *Handbuch der Physik* (Springer, Berlin, 1967).
[46] P. Souvatzis, O. Eriksson, M. I. Katsnelson, and S. P. Rudin, Phys. Rev. Lett. **100**, 095901 (2008).
[47] O. Hellman, I. A. Abrikosov, and S. I. Simak, Phys. Rev. B **84**, 180301(R) (2011).
[48] V. L. Moruzzi, J. F. Janak, and K. Schwarz, Phys. Rev. B **37**, 790 (1988).
[49] M. A. Blanco, E. Francisco, and V. Luaña, Comput. Phys. Commun. **158**, 57 (2004).
[50] C. Toher, J. J. Plata, O. Levy, M. de Jong, M. Asta, M. B. Nardelli, and S. Curtarolo, Phys. Rev. B **90**, 174107 (2014).
[51] B.-C. Zhou, S.-L. Shang, and Z.-K. Liu, Acta Mater. **103**, 573 (2016).
[52] C.-M. Li, Q.-M. Hu, R. Yang, B. Johansson, and L. Vitos, Phys. Rev. B **91**, 174112 (2015).
[53] D. Ma, B. Grabowski, F. Körmann, J. Neugebauer, and D. Raabe, Acta Mater. **100**, 90 (2015).
[54] Z.-G. Mei, S.-L. Shang, Y. Wang, and Z.-K. Liu, Phys. Rev. B **80**, 104116 (2009).
[55] C.-E. Hu, Z.-Y. Zeng, L. Zhang, X.-R. Chen, L.-C. Cai, and Alfè, J. Appl. Phys. **107**, 093509 (2010).
[56] P. Debye, Ann. Phys. **39**, 789 (1912).
[57] J. C. Slater, *Introduction to Chemical Physics* (McGraw-Hill, New York, 1939).
[58] Z.-J. Wu, E.-J. Zhao, H.-P. Xiang, X.-F. Hao, X.-J. Liu, and J. Meng, Phys. Rev. B **76**, 054115 (2007).
[59] W. Voigt, *Lehrbuch der Kristallphysik* (Teubner, Leipzig, 1928).
[60] A. Reuss, Z. Angew. Math. Mech. **9**, 49 (1929).
[61] R. Hill, Proc. Phys. Soc., London, Sect. A **65**, 350 (1952).
[62] D. G. Pettifor, *Bonding and Structure of Molecules and Solids* (Clarendon, Oxford, 1995).
[63] A. Paulsen, J. Frenzel, and G. Eggeler (private communication).
[64] L.-F. Huang, B. Grabowski, J. Zhang, M.-J. Lai, C. C. Tasan, S. Sandlöbes, D. Raabe, and J. Neugebauer, Acta Mater. **113**, 311 (2016).
[65] S. Barzilai, C. Toher, S. Curtarolo, and O. Levy, Acta Mater. **120**, 255 (2016).
[66] B. Xiao, J. Feng, C. T. Zhou, Y. H. Jiang, and R. Zhou, J. Appl. Phys. **109**, 023507 (2011).
[67] D. Connétable and O. Thomas, Phys. Rev. B **79**, 094101 (2009).